

# ANTIPARTICLE TO PARTICLE RATIOS OF STRANGE BARYONS AT RHIC

XinXin Du, Wellesley College, UCLA REU 2004

Strangeness measurements provide information about the dynamics of a system created by heavy ion collisions. We analyzed data for  $\Lambda$ ,  $\Xi$ , and  $\Omega$  production for dAu collisions at 200GeV and AuAu collisions at 62 GeV. We conclude that the antiparticle to particle ratios for these particles increase as the strangeness content increases. The ratios also increase as the energy of the collisions increase.

## Introduction and Background

At RHIC (Relativistic Heavy-Ion Collider), heavy ions such as  $Au^{79+}$  collide at relativistic speeds of up to  $\gamma = 100$ . Each nucleon at this speed has energy of approximately 100 GeV. If two ions of mass 200 GeV each collide at  $\gamma = 100$ , the energy of the collision could reach a maximum of 40000 GeV. Although the energy transferred from a collision would usually reach only a small fraction of the maximum energy, that small part of energy is enough to create many new particles. Collisions of heavy ions with energies of this order of magnitude result in the creation of many quarks within a very small volume. This high density of quarks could briefly form quark gluon plasma (QGP), a phase of matter in which quarks are deconfined. [ref 4].

Since there are no strange quarks in the colliding particles, we know that all the strange quarks that appear in particles after the collision are produced from the lost energy of the inelastic collision. The temperature of the collision system at RHIC can be as high as 150 MeV, which is greater than the theoretical QGP temperature which is approximately 120 MeV. We know that this temperature provides enough energy to produce quark-anti-quark pairs from gluon-gluon interactions; and gluon-gluon pair production requires less energy than the threshold energy for producing strange particles and antiparticles by associated production. Thus, if a QGP

state exists in this collision system, then gluon-gluon interactions is the dominant strange quark production mechanism, and pair production is the dominant strange particle production mechanism in QGP. Thus strange antiparticle to particle ratios increase and strange particle yield increases if there is QGP. With lower energy threshold, strange quarks are easier and therefore more abundantly produced in QGP; this is strangeness enhancement. We can also ask the question whether the collision is net baryon free, as well as find the pair production to total production ratio of strange particles. [Ref. 4]

In this paper, I will discuss my results for antiparticle to particle ratios for the strange baryons  $\Lambda$ ,  $\Xi$ , and  $\Omega$  for deuteron on gold collisions at  $\sqrt{s} = 200GeV$  and for gold on gold collisions at  $\sqrt{s} = 62GeV$ . I will describe the procedure that I used to obtain the results, as well as conclude that the antiparticle to particle ratios for strange baryons increase with the strangeness content of the particles, and they increase with the energy of the collision.

## Procedure to Find the Antiparticle to Particle Ratios of $\Lambda$ , $\Xi$ , and $\Omega$

### Outline of Procedure

This STAR detector detects a large number of particle tracks that leave the collision. The particles that form these tracks are charged particles that ionize the

gas in the gas chamber of the detector. The electric field inside the detector causes the ionized electrons in the gas to drift to the ends of the detector where they are detected. The magnetic field inside the detector causes the charged particle tracks to travel a helical path that is circular in the x-y plane and has a constant velocity in the z direction.

Since strange baryons decay before they reach the detector, we need to count them by looking at their decay products, which are charged kaons, pions, and protons. A  $\Lambda$  decays by the process  $\Lambda \rightarrow p^+ + \pi^-$ . A  $\Xi$  decays by the process  $\Xi \rightarrow \pi^- + \Lambda$  from which the  $\Lambda$  decays by its own decay process. An  $\Omega$  decays by the process  $\Omega \rightarrow K^- + \Lambda$  from which the  $\Lambda$  decays by its own decay process. We count the numbers of  $\Lambda$ ,  $\Xi$ , and  $\Omega$  by reconstructing these particle masses from their decay products according to the invariant mass equation:

$$E^2 = \mathbf{p} \bullet \mathbf{p} + m^2 \quad (1)$$

which holds for any particle.

### Details of Procedure

We can use the reconstruction of  $\Lambda$  as an example for this discussion. A  $\Lambda$  decays into a  $p^+$  and a  $\pi^-$  whose tracks are easily detected by the detector. The procedure for  $\Lambda$  construction is as follows:

We take pion and proton tracks that are in the vicinity of each other and assume that they are the decay products of the same  $\Lambda$ . We can use momentum and energy conservation to compute the momentum and energy of the assumed  $\Lambda$  because  $p_\Lambda = p_p + p_\pi$  and  $E_\Lambda = E_p + E_\pi$ . From  $p_\Lambda$  and  $E_\Lambda$ , we can compute the mass of the assumed  $\Lambda$ . We can then make a histogram of the masses of all the assumed  $\Lambda$ s. This mass histogram will have a peak at the mass of  $\Lambda$ , 1.115 GeV (Fig.1). The background of the mass histogram comes from the combinatorics of the reconstruction. The integration of this peak will give us the number of  $\Lambda$ s in a particular collision (assuming that the detector detects all the pions and protons that come out of the collision).

If we do the same for  $\bar{\Lambda}$ , then we can count the number of  $\bar{\Lambda}$ s produced in the collision. If we assume the same reconstruction efficiency for  $\bar{\Lambda}$ , then this will

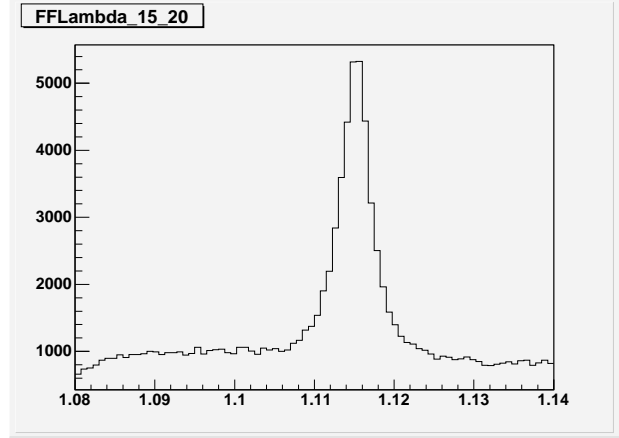


Figure 1: Mass histogram for  $\Lambda$  at  $p_T$  bin 1.5 to 2.0.

give us the ratio of  $\frac{\bar{\Lambda}}{\Lambda}$  for the collision. We can do the same for  $\Xi$  and  $\Omega$ .

### Procedure to find $p_T$ and $p_z$

We take the z direction as the direction along the detector and the x-y plane as the cross-sectional plane to the detector. The transverse momentum of any detected particle is computed by:

$$\frac{mv_T^2}{R} = qv_TB \quad (2)$$

from which we obtain

$$p_T = RqB \quad (3)$$

We also know that in the time  $\Delta t$ , the ratio of the arc-length traveled by the particle to the distance it travels in the z direction is equal to the ratio of  $p_T$  to  $p_z$ . Thus we can obtain  $p_z$ .

### Integration and Background: Methods, Precautions, and Problems

The integration of the mass peak is found by fitting the peak and background to a Gaussian and a straight

line. The form of the fitting equation is:

$$Ae^{\frac{(x-b)^2}{2c^2}} + Dx + E \quad (4)$$

One way to find the  $\Lambda$  yield in the peak is to integrate the Gaussian. This method did not to give very accurate results since the peak was not a purely statistical peak and thus was not a good Gaussian. A better method was to integrate the mass histogram in a small mass region around the peak and subtract the integration of the background fit in that region. This gave more accurate results.

To control the amount of background or signal on a particular histogram, one could apply stricter or more relaxed geometric cuts on the particle reconstruction. For the  $\Omega$  particle, finding proper geometric cuts for the mass histogram was particularly important since the  $\Omega$  signal was so small. One also must be sure to use the same geometric cuts for antiparticles as particles in order to ensure that the ratio computed is meaningful.

Another way to reduce the background readings is to recompute the mass histogram of a particle for a particular collision by first rotating all the tracks made by positive charges in the collision by 180 degrees. This new histogram will have only background, no peak. We then normalize this new histogram to the same magnitude as the background of the histogram that contains the peak, and subtract the new histogram from the one with a peak. This method is good if the signal is very, very weak, such as the case in the reconstruction of the pentaquark.

## Results and Errors

I obtained the results for the ratios  $\frac{\bar{\Lambda}}{\bar{\Lambda}}$ ,  $\frac{\bar{\Xi}}{\bar{\Xi}}$ , and  $\frac{\bar{\Omega}}{\bar{\Omega}}$  for dAu collisions at 200 GeV for forward field, reversed field, and combined fields, and I took the combined field results as the final ratio results. I also obtained the ratio results for the same particles for AuAu collisions at 62 GeV for the reversed field.

Forward and reversed field refer to the direction of the magnetic field inside the detector. Particle ratios should not change when the field is reversed. Thus, for the 200 GeV collisions, I took as systematic error the discrepancy in ratios between the forward and

reversed field collisions. The antiparticle to particle ratios are binned according to  $p_T$ , the computed transverse momentum of the particles. We expect that the ratios are constant across  $p_T$  for the  $p_T$  region 0 to 4. The statistical errors are related to the particle yield as  $\sqrt{N}$ , where  $N$  is the particle yield. The total error is computed as the square root of the sum of the squares of the systematic error and the statistical error.

Because the theoretical treatment for collisions at low  $p_T$  is different from collisions at high  $p_T$ , we always bin according to  $p_T$  and talk about the  $p_T$  spectrum of some particle. Fig.2 is an example of a  $p_T$  spectrum for the  $\Lambda$  and  $\bar{\Lambda}$  particle yields from the 62 GeV dAu collisions that I analyzed. Fig.3 is the ratio of  $\frac{\bar{\Lambda}}{\Lambda}$  as a function of  $p_T$ ; note that this ratio is mostly flat across  $p_T$ . Fig.4 and Fig.5 are similar plots for the  $\Xi$ s.

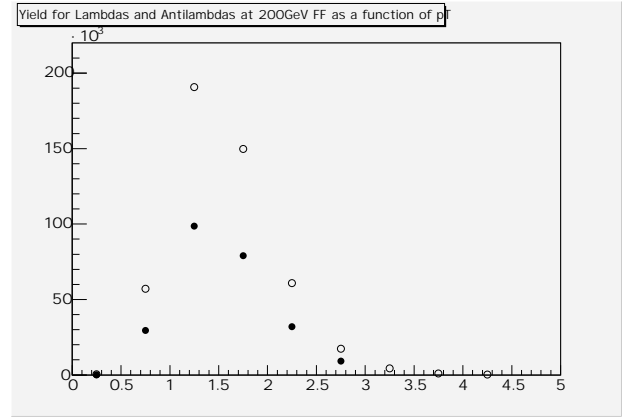


Figure 2:  $\circ = \Lambda$ ,  $\bullet = \bar{\Lambda}$ .  $p_T$  spectrum for  $\Lambda$  and  $\bar{\Lambda}$  particle yields.

For the 200 GeV dAu collisions, the combined field results are:  $\frac{\bar{\Lambda}}{\Lambda} = 0.79 \pm 0.1$ ,  $\frac{\bar{\Xi}}{\Xi} = 0.77 \pm 0.8$ , and  $\frac{\bar{\Omega}}{\Omega} = 0.9 \pm 0.2$ . The results for  $\Lambda$  and  $\Xi$  are obtained by averaging over six  $p_T$  bins with total  $p_T$  range from 1 to 4 and bin width 0.5. The result for  $\Omega$  is obtained from the average of two  $p_T$  bins with total  $p_T$  range from 0.5 to 3.5 and bin width 1.5.

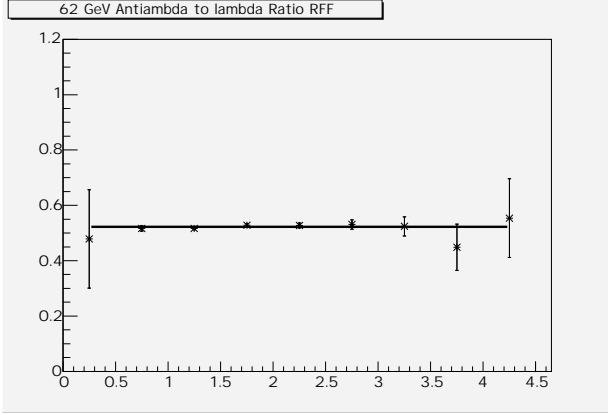


Figure 3:  $\bar{\Lambda}$  to  $\Lambda$  ratio as a function of  $p_T$  for the 200 GeV dAu collision. The line is the line of best fit for the data points, considering error. The line is very flat across  $p_T$ .

For the 62 GeV AuAu collisions, the reversed field results are:  $\frac{\bar{\Lambda}}{\Lambda} = 0.523 \pm 0.003$ ,  $\frac{\bar{\Xi}}{\Xi} = 0.66 \pm 0.01$ , and  $\frac{\bar{\Omega}}{\Omega} = 0.8 \pm 0.2$ . The results for  $\Lambda$  was obtained by an average over 9  $p_T$  bins, with total  $p_T$  range from 0 to 4.5. The  $\Xi$  result was obtained by an average over 7  $p_T$  bins with total  $p_T$  range from 0 to 1. The  $\Omega$  result was the the ratio for a single  $p_T$  bin that ranged from 1.5 to 2.5.

Fig. 4 and Fig.5 show the plots for the antiparticle to particle ratios for the three particles graphed according to mass for the 200 GeV and 62 GeV collisions.

We note that the ratios increase as a function of mass, i.e. the ratios increase as a function of the strangeness content of the particle.

Using results from earlier analysis from the STAR group for AuAu collisions at 130 GeV and at 200 GeV, we can look at the relationship between antiparticle to particle ratios as a function of collision energy as in the graph in Fig.6:

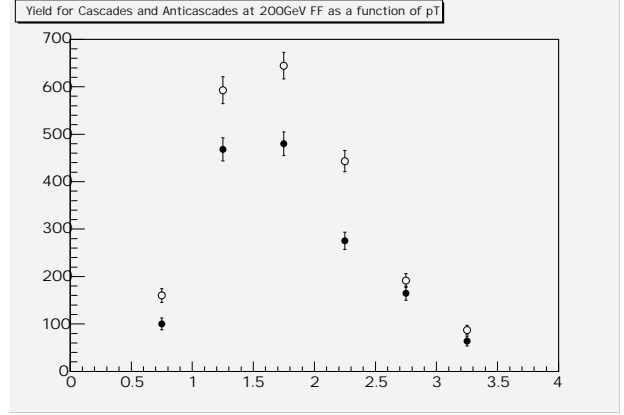


Figure 4:  $\circ = \Xi$ ,  $\bullet = \bar{\Xi}$ .  $p_T$  spectrum for  $\Xi$  and  $\bar{\Xi}$  particle yields.

## Conclusions

Since most of these particle ratios are approximately between 0.6 and 0.8, then we conclude that collisions of these energies have a ratio of approximately 2/3 for the pair production to total production of strange particles. Since the ratios found for these collisions are less than 1, we can say that the collisions are not net baryon free. We can conclude that antiparticle to particle ratios increase as a function of the strangeness content of the particles. We can also say that the ratios increase as a function of the collision energy.

## Acknowledgments

I would like to thank Dr. Hui Long, Professor Huan Huang, and Professor Charles Whitten for advising me on this project. I thank Françoise Queval for coordinating the REU program, and I thank the NSF for funding this research.

## References

- [1] B.B. Back et al., Phys. Rev. Lett. **87**,10 (2001).

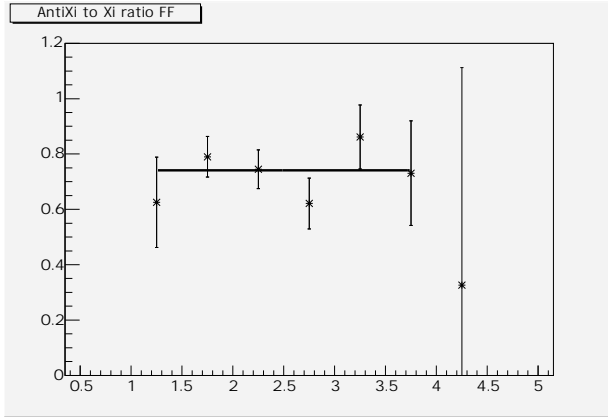


Figure 5:  $\bar{\Xi}$  to  $\Xi$  ratio as a function of  $p_T$  for the 200 GeV dAu collision. The line is the line of best fit for the data points, considering error.

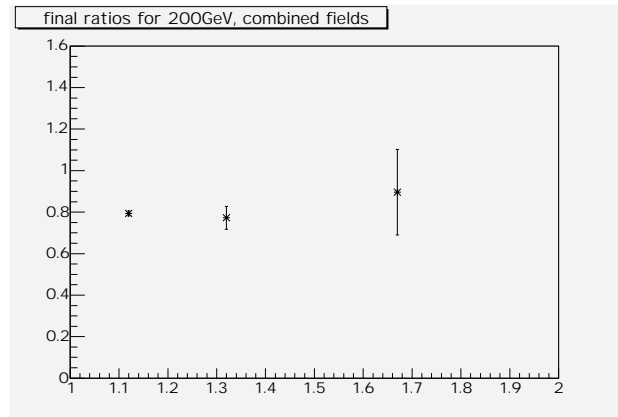


Figure 6: Antiparticle to particle ratios as a function of particle mass for the 200 GeV dAu collisions.

- [2] C.Adler et al., nucl-ex/0104022 v1, 23 Apr 2001; nucl-ex/0203016 v1, 22 Mar 2002.
- [3] J.Adams et al., nucl-ex/0211024 v2, 15 Jul 2003.
- [4] Wong, Cheuk-Yin, *Introduction to High-Energy Heavy-Ion Collisions* (World Scientific, Singapore, 1994).
- [5] Perkins, Donald H. *Introduction to High-Energy Physics* (Addison-Wesley Publishing Company, Inc., California, 1987).

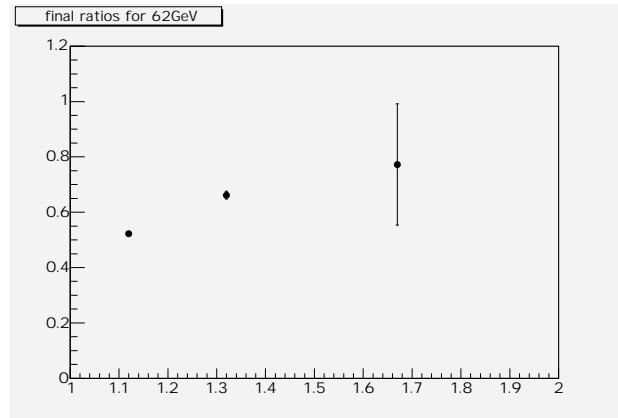


Figure 7: Antiparticle to particle ratios as a function of particle mass for the 62 GeV AuAu collisions.

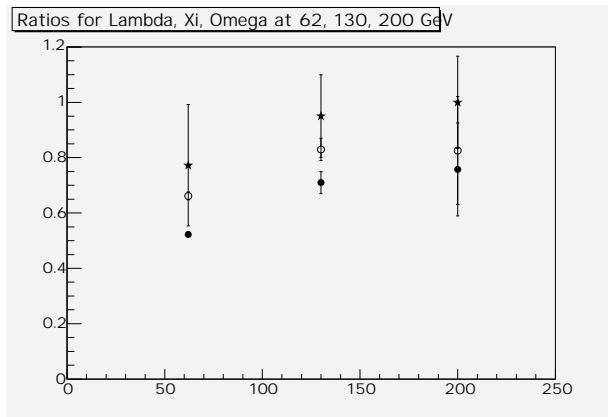


Figure 8: ● =  $\frac{\bar{\Lambda}}{\Lambda}$ , ○ =  $\frac{\bar{\Xi}}{\Xi}$ , ★ =  $\frac{\bar{\Omega}}{\Omega}$ . Ratio results for  $\Lambda$ ,  $\Xi$ , and  $\Omega$  at 62 GeV, 130 GeV (reference, and 200 GeV. Note that ratios increase with strangeness as well as collision energy